Preprint Title	Enhanced cell target specificity and uptake of lipid nanoparticles using RNA aptamers and peptides
Authors	Roslyn M. Ray, Anders H. Hansen, Maria Taskova, Bernhard Jandl, Jonas Hansen, Citra Soemardy, Kevin V. Morris and Kira Astakhova
Publication Date	26 Jan. 2021
Article Type	Full Research Paper
Supporting Information File 1	Supporting Information.docx; 3.1 MB
ORCID® iDs	Maria Taskova - https://orcid.org/0000-0002-9727-2496; Kira Astakhova - https://orcid.org/0000-0003-4878-0301

Enhanced cell target specificity and uptake of lipid nanoparticles using RNA aptamers and peptides

Roslyn M. Ray[‡1], Anders Højgaard Hansen[‡2], Maria Taskova[2], Bernhard Jandl,[3] Jonas Hansen,[2] Citra Soemardy[1], Kevin V. Morris[1,4], Kira Astakhova*[2]

Email: Kira Astakhova - kiraas@kemi.dtu.dk

* Corresponding author

‡ Equal contributors

[1] The Center for Gene Therapy, The Beckman Research Institute, The City of Hope, Duarte CA, [2] The Department of Chemistry, Technical University of Denmark, Lyngby Denmark, [3] Institute of Biological Chemistry, Faculty of Chemistry, University of Vienna, 1090 Vienna, Austria and [4] School of Medical Sciences, Griffith University and the Menzies Health Institute Queensland, Gold Coast, Australia 4222.

Abstract

Lipid nanoparticles (LNPs) constitute a facile and scalable approach for delivery of payloads to human cells. LNPs are relatively immunologically inert and can be produced in a cost effective and scalable manner. However, targeting and delivery of LNPs across the blood brain barrier (BBB) has proven challenging. In an effort to target LNPs to particular cell types as well as generating LNPs that can cross the BBB, we developed and assessed two approaches whereby BBB penetrating peptides Tat or T7, and RNA aptamers targeted to gp160 from HIV or CCR5, a HIV-1 co-receptor, were incorporated into LNPs. We report here that a CCR5 selective RNA aptamer acts to facilitate entry through a simplified BBB model and to drive the uptake of LNPs

into CCR5 expressing cells, while the gp160 aptamer did not. We further observed that the addition of cell penetrating peptides, Tat, did not increase BBB penetration above the aptamer loaded LNPs alone. Moreover, we find that these targeted LNPs exhibit low immunogenic and low toxic profiles and that targeted LNPs can traverse the BBB to potentially deliver drugs into the target tissue. This approach highlights the usefulness of aptamer loaded LNPs to increase target cell specificity and potentially, deliverability across the BBB.

Keywords

Lipid nanoparticle; aptamer; blood-brain-barrier; gene therapy; HIV-1

Introduction

Lipid nanoparticles (LNPs) represent an effective platform for delivering of small molecules, RNA or DNA into target cells [1]. LNPs have been successfully deployed via different administration routes *in vivo* to distribute their cargo into target tissues [2-8]. By changing lipid composition [6] and/or including short peptides [9] and ligands [10], one can modulate the biodistribution of the LNP in the body. However, despite these advances, targeting of LNPs to the brain tissue remains a challenge [11].

In order to reach safer therapeutic options for treatment of brain diseases and disorders, a productive drug transport across the blood-brain-barrier (BBB) is critical. For example, despite successful implementation of antiretroviral drugs for the treatment of human immunodeficiency virus (HIV-1), HIV-1 associated neurological disorders persist due to the poor uptake of antiretroviral drugs across the BBB [12-14]. There are two ways to traverse the BBB, one is through temporary disruption of the physical barrier, that impairs BBB function, the other is to

use nanocarriers or particles [11]. The latter presents a non-invasive route that is safer than physical disruption [11]. One approach to increase transport of LNPs through the notoriously protective BBB is to use short positively charged peptides or receptor specific ligands, both of which have shown to be effective at increasing transport of LNPs, nucleotides and small molecules through the BBB [9, 15-17]. For example, the short positively charged peptide, Tat, has previously been demonstrated effective as an excipient species to increase the uptake through the negatively charged BBB [9, 18]. Tat (H-YGRKKRRQRRR-NH_2) is an arginine rich short cell penetrating peptide derived from the natural nuclear trans-activator of transcription (Tat) protein of HIV-1 [19, 20]. The HIV-1 Tat protein itself, has been shown to traverse the BBB by acting as a cell-penetrating peptide [9, 20]. Other small positively charged molecules used for BBB penetration is transferrin and its peptide derivatives or analogs that act as ligands for the transferrin receptor. The transferrin receptor is highly expressed in brain capillaries, nucleated cells and in rapidly dividing cells [21], and its endogenous ligand transferrin, has previously been used to increase transport of small molecules and oligonucleotides across the BBB [21-23]. The seven-amino-acid peptide T7 (H-HAIYPRH-NH_2) was identified via phage display [24] and has a high affinity (~10 nM) for the transferrin receptor [24, 25]. This peptide does not compete with endogenous transferrin binding and has been used to successfully enhance the drug delivery to brain tissue [15, 22, 24-26]. Both peptides were included in this study and modified with an N-terminal lipid anchor for LNP post-insertion. The design of the lipid anchor includes two palmitoyl chains that are attached through a 1,2-diamino propanoic acid (Dap) moiety on the N-terminus of each peptide, providing the lipopeptides dipalmitoyl-Dap-T7 and dipalmitoyl-Dap-Tat. Double lipidation ensures a more stable lipid membrane anchoring compared to a single fatty acid chain or cholesteryl variant [27-29]. The careful choice of Dap

and palmitic acid allows for the entire synthesis to be performed on solid support with no need for additional reactions after cleavage [27-29].

One approach to generate LNP formulations with higher specificity for antigen-expressing cells is to use RNA aptamers. RNA aptamers are short oligonucleotides that are evolved using a process called Systematic Evolution of Ligands by Exponential Enrichment (SELEX) [30]. SELEX is an iterative process that begins with a large oligonucleotide library which, through a process of negative and positive selection, ends with a few candidates that are specific for a particular protein [30, 31]. Using HIV-1 as our model, we explored the use of two RNA aptamers as a mean to increase the specificity of LNPs for HIV-1 infected and/or target cells [31]. RNA aptamers are ideal candidates due to their lower immunogenicity profile than their DNA counterparts [30, 32, 33]. RNA aptamers are also highly amenable to forming complex and dynamic secondary structures that makes them ideal molecules for novel ligand development [31]. Zhou et al., previously reported on an RNA aptamer specific for the HIV-1 entry co-receptor C-C chemokine receptor type 5 (CCR5) [34] and an RNA aptamer specific for the HIV-1 envelope protein gp160 [35]. The CCR5 RNA aptamer G-3, has been shown to be specific for and internalized by the CCR5 receptor [34]. Similarly, the A-1 aptamer has been found to specifically recognize gp160 and that it may be internalized through receptor-mediated endocytosis [35]. Thus, both aptamers present an additional potential route for LNP internalization and target cell specificity. In order to assess the ability of aptamers to drive LNP internalization, short complementary Cy5-DNA oligonucleotides specific for each aptamer were used as probes to detect LNP uptake in different cells.

In this study, we employed lipid compositions and formulation procedures previously reported in literature [4]. Specifically, the cationic and ionizable DLin-MC3-DMA lipid is a constituent of the FDA-approved LNP-formulated small interfering RNA (siRNA) drug Patisiran® for treatment of

familial transthyretin amyloidosis [36, 37]. Clinical trial safety assessments of this formulation showed no liver toxicity and no immune stimulation with ~10% of trial participants experiencing mild to moderate adverse events upon administration [38]. It includes encapsulation of siRNA by a mixture of lipid components such as an ionizable cationic lipid, distearolyphosphatidycholine (DSPC), cholesterol and PEG-lipid, each with an essential role in the design. These lipids promote the effective distribution of the LNP *in vivo* as well as aide in effective cargo release from the endosome [1, 37].

To this end, we herein report the efficacy, delivery capability and functionality of the addition of peptides and RNA aptamers in facilitating entry through a simplified BBB model as well as to determine whether inclusion of these molecules could facilitate cell specific uptake. We further show that LNPs generally exhibit a low immunogenic and toxic profile and that RNA aptamers can act as potential enhancers to effectuate the delivery of LNPs into the CNS.

Results

Lipid nanoparticle development and characteristics

In accordance with a previously published procedure, we generated LNPs using a mixture of DLin-MC3-DMA, DSPC, cholesterol and DMG-PEG 2000. Lipids were first extruded then complexed with negatively charged aptamers annealed with fluorescently tagged complementary DNA oligonucleotides (GP160:A-1 or CCR5:G-3) to simultaneously assemble the LNPs. At this stage, the LNPs were examined by DLS (**Table 1**). While non-complexed (empty) LNPs had an average size of 62.4 nm and zeta potential (ZP) of -2.9 mV, LNPs mixed with GP160:A-1 and CCR5:G-3 displayed average sizes of 57.3 nm and 91.9 nm, and more negative ZPs (-11 mV and -9.4 mV), respectively (**Table 1**). These ZP values indicate that complexation leads to a neutral to anionic LNP product[39], properties that typically confer with

low to no cytotoxicity *in vivo* [40]. Further, the additional decrease in the ZP indicates efficient aptamer loading into the LNPs. Additionally, low polydispersity index (PDI) values is reported for both formulations (**Table 1**) indicating a relative high degree of monodispersity.

Sample list: Listed samples used in present study.

LNP sample	**Cy5 DNA probe:aptamer**	**Lipopeptide**
LNP B9	-	-
LNP B9 A-1	A-1:GP160	-
LNP B9 G-3	G-3:CCR5	-
LNP B9 T7	-	T7
LNP B9 Tat	-	Tat
LNP B9 A-1 T7	A-1:GP160	T7
LNP B9 A-1 Tat	A-1:GP160	Tat
LNP B9 G-3 T7	G-3:CCR5	T7
LNP B9 G-3 Tat	G-3:CCR5	Tat

Table 1: DLS data listing particle size, polydispersity index (PDI), and zeta potential (ZP) of LNP formulations. For sample composition, see sample list, above.

LNP formulation	**Physical characterization by DLS**	
LNP B9	Mean diameter PDI ZP	62.4 ± 0.7 nm 0.2 ± 0.01 -2.9 ± 1.1 mV
LNP B9 A-1	Mean diameter PDI ZP	57.3 ± 0.9 nm 0.1 ± 0.03 -11.0 ± 1.4 mV
LNP B9 G-3	Mean diameter	91.9 ± 4.2 nm

	PDI	0.3 ± 0.03
	ZP	-9.4 ± 1.0 mV

Next, LNPs were incubated with either Tat or T7 and the physical characteristics assessed by nanoparticle tracking analysis (NTA) (**Table 2**) and TEM (**Supplementary Figure S2)**. After post-insertion, LNP sizes were found by NTA to range from 54–66 nm (**Table 2**), while TEM analysis revealed average sizes between 45–52 nm (**Supplementary Figure 2B**). While there appears to be a ~10 nm discrepancy when comparing DLS and NTA with TEM, this size difference was found to be consistent between method of analysis for all sample.

For example, LNP B9 T7 was characterized by the smallest average size using both NTA (~54 nm) and TEM (~45 nm). Thus, the average sizes obtained by NTA are in agreement with the average size observed using TEM (**Supplementary Figure 2A and Table 2**). Similarly, while the mean diameter of LNP B9 G-3 was found to be larger by DLS (91.1 nm) than the values reported for NTA (67.2 nm) and TEM (52 nm), the sizes of the LNP B9 and LNP B9 A-1 samples via DLS are also in agreement with the NTA and TEM reported sizes. These discrepancies may be indicative of the inherent differences between these three analysis methods and highlight the need to confirm LNP sizes using more than one technique. Nevertheless, the small size of these nanoparticles (<100 nm) is ideal for *in vivo* applications as they may bypass the reticuloendothelial system and thereby increase LNP circulation time *in vivo* [41].

Table 2: NTA analysis showing Size and Concentration of LNPs. For sample composition, see sample list, above.

Sample Name	Physical characterization by NTA	
LNP B9	Mean diameter	69.2 ± 0.3 nm
	SD	30.8 ± 1.5 nm
	Concentration	$3.13 \cdot 10^{11} \pm 1.75 \cdot 10^{10}$ particles/mL
LNP B9 A-1	Mean diameter	66.6 ± 1.4 nm
	SD	25.2 ± 1.4 nm

	Concentration	3.82e+011 ± 6.20e+009 particles/mL
LNP B9 A-1 T7	Mean diameter	Mean: 65.7 ± 1.1 nm
	SD	SD: 26.3 ± 2.4 nm
	Concentration	3.25e+011 ± 2.82e+010 particles/mL
LNP B9 A-1 Tat	Mean diameter	54.2 ± 0.6 nm
	SD	22.1 ± 1.4 nm
	Concentration	8.90e+11 ± 7.23e+10 particles/mL
LNP B9 G-3	Mean diameter	67.2 ± 0.3 nm
	SD	30.2 ± 0.8 nm
	Concentration	2.71e+011 ± 1.45e+010 particles/mL
LNP B9 G-3 T7	Mean diameter	66.5 ± 1.7 nm
	SD	32.2 ± 5.0 nm
	Concentration	3.30e+011 ± 2.60e+010 particles/mL
LNP B9 G-3 Tat	Mean diameter	57.3 ± 0.5 nm
	SD	29.2 ± 1.7 nm
	Concentration	8.05e+11 ± 7.83e+10 particles/mL
LNP B9 T7	Mean diameter	75.1 ± 1.5 nm
	SD	32.0 ± 1.4 nm
	Concentration	2.19e+011 ± 1.65e+010 particles/mL
LNP B9 Tat	Mean diameter	61.2 ± 0.7 nm
	SD	15.2 ± 1.5 nm
	Concentration	2.19e+11 ± 1.69e+10 particles/mL

LNPs with post-insertion T7 peptide

Previous studies have demonstrated the ability of the T7 peptide to increase LNP transport across the blood brain barrier (BBB) [22-24, 42]. In order to test this, we used a simple transwell assay with human brain endothelial cells (hCMEC/D3) that were cultured on a 0.4 µM transwell mesh until a trans-endothelial electrical resistance of above 30 $\Omega.cm^2$ was reached. This measure is an indicator that a tight junction barrier has formed within these cells and can be used to determine the ability of the LNPs to pass through the BBB (**Supplementary Figure 3A**). Additionally, we further confirmed our junctions using fluorescent microscopy on the barrier layers to confirm expression of claudin-5, a known tight junction protein (**Supplementary Figure 3B**). We observed that LNPs were readily taken up by both HeLa and TZM-bls in the absence

of a transwell insert (**Figure 1A-B**). With the addition of the hCMEC/D3 cells in the apical chamber, we found that HeLa cells were less Cy5 positive (~60%) than the target TZM-bl cells (~100%) (**Figure 1A**). Further, when examining the intensity of Cy5 in these cell populations, we found that the addition of the T7 peptide increases uptake by 1.2 fold through the hCMEC/D3 cellular barrier, while also increasing uptake through direct addition by 1.6 - 1.8 fold (**Figure 1B**). Additionally, the mean fluorescent intensity (MFI) was found to be 2–2.3 fold higher in the target TZM-bl cells in both barrier and non-barrier treatment groups, compared to the control HeLa cells, indicating a higher accumulation of LNPs in the target cells (**Figure 1B, Supplementary Figure 4**). Passive diffusion of the LNPs with the G-3 aptamer alone through a transwell insert without hCMEC/D3 cells appears to show higher uptake in the HeLa cell line but lower uptake in the TZMbl cell line in comparison to the transwell insert with hCMEC/D3 cells (**Figure 1A-B**). In contrast, we found that formulating LNPs with the gp160 specific A-1 aptamer did not result in any significant increase in percentage uptake in the target gp160 positive HEK293T cells compared to HEK293T cells alone (**Figure 1C**). However, we did observe that the MFI in gp160 positive HEK293T to be 1.3 and 1.45 fold (barrier, and non-barrier groups respectively) higher than in the HEK293T cells alone (**Figure 1D**), suggesting higher levels of LNPs in gp160 expressing HEK293T cells. We also observed that direct addition of the LNPs resulted in a higher percentage of Cy5 positive cell detection and a higher MFI compared to the hCMEC/D3 barrier (**Figure 1D, Supplementary Figure 4**).

Collectively, these data suggest that the candidate LNPs, particularly the LNP B9 G-3 T7, may increase uptake through tight junctions and prove useful in transiting drugs and small cargo through the BBB *in vivo*.

Figure 1

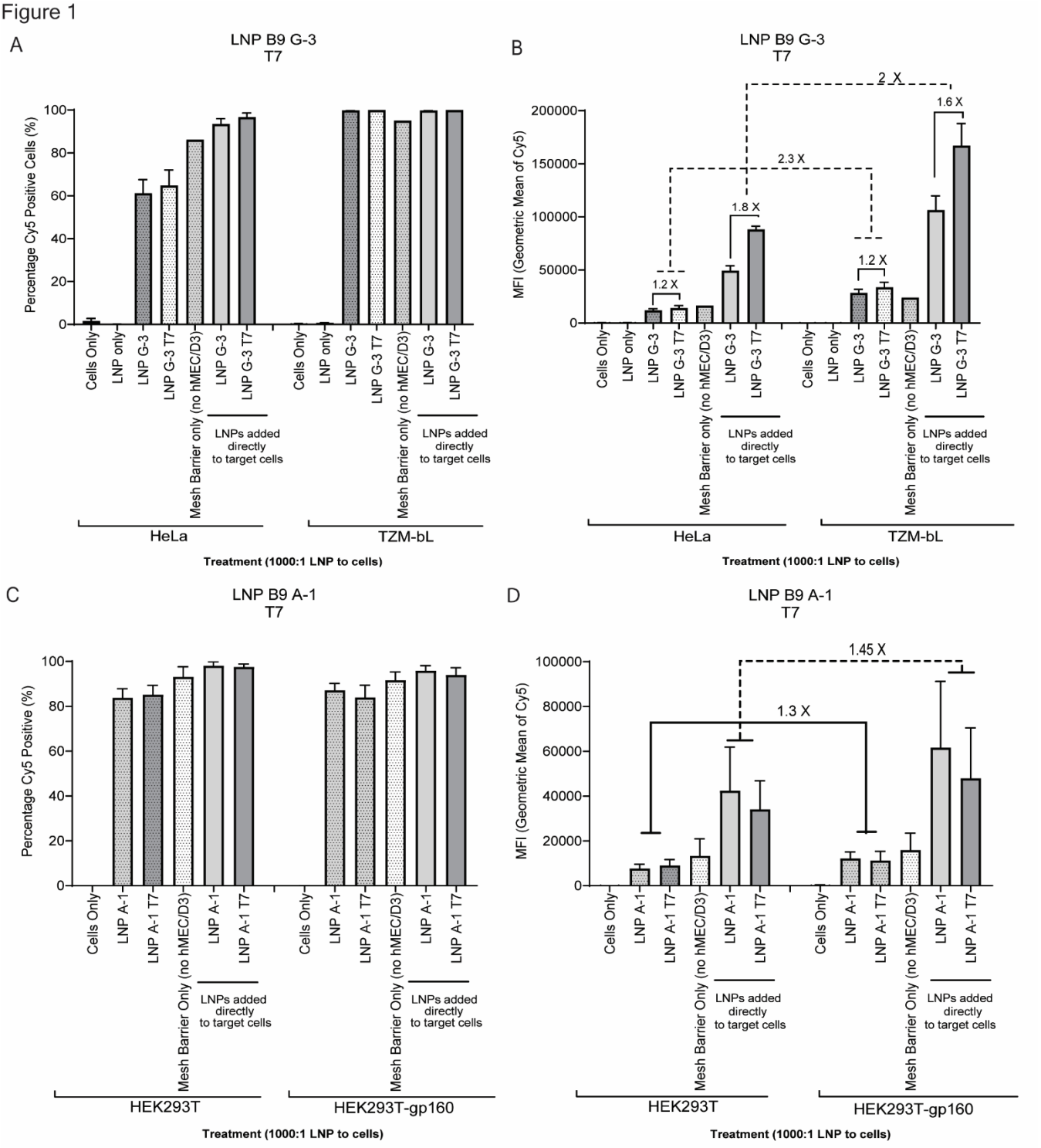

Figure 1: LNPs with T7 pass through the transwell cell barrier and are taken up by target cells. (A-B) HeLa (CCR5 negative control cell) or TZM-bl (CCR5 positive cell type) and (C-D) HEK293T or gp160 positive HEK293T cells were seeded at a density of 50 000 cells/24well. The

next day, transwell inserts containing confluent hMEC/D3 cells at TEERs above 30 Ω.cm^2 were placed into experimental wells, LNPs (1000:1) were added to the apical surface and 24 hours later, the target cells were processed for Cy5 detection using slow assisted cytometry (FACs). (A) Percentage cells positive for Cy5 detection in HeLa and TZM-bls (B) Mean fluorescent intensity of Cy5 in each cell population in HeLa and TZM-bls. (C) Percentage cells positive for Cy5 detection in HEK cell types (B) Mean fluorescent intensity of Cy5 in each cell population in HEK cell types. Histograms are representative of three independent biological experiments, each containing duplicate technical replicates.

LNPs with post-inserted Tat peptide

Tat is a cationic peptide that is known to increase transport of molecules through the blood brain barrier and increase uptake into cells [18]. In a similar manner to the transferrin peptide (T7), we investigated the ability of Tat to drive LNP uptake in cell lines. Interestingly, we found that the addition of the Tat peptide to either the A-1 or G-3 complexed LNPs did not have any effect on BBB penetration (**Figure 2 A-D**). Rather, we observed that LNPs containing the G-3 aptamer showed an increase uptake in target cells expressing CCR5 (**Figure 2 A-B**). We observed that TZM-bls had a ~98% uptake of LNPs via the hCMEC/D3 barrier compared to ~63% in HeLa cells (**Figure 2A**). We also observed a similar increase (1.75 fold, barrier and 1.65 fold, non-barrier) in MFI in TZM-bl target cells compared to the non-target HeLa cells (**Figure 2B, Supplementary Figure 4**). Further, we observed similar trends for the A-1 aptamer, where Tat had no effect on BBB penetration (**Figure 2 C-D, Supplementary Figure 4**). Interestingly, in this group, percentage uptake was lower across all groups, compared to the LNP A-1 T7 group (**Figure 1 C-D**). This may be due to differences in hCMEC/D3 barrier formation or LNP counting error using NTA.

Collectively, these data suggest that the addition of Tat to LNPs have no effects on BBB transit when compared to the T7 peptide. We further found that A-1 aptamer incorporation into the LNP formulation does not appear to enhance specific targeting of gp160 expressing cells either

Figure 2

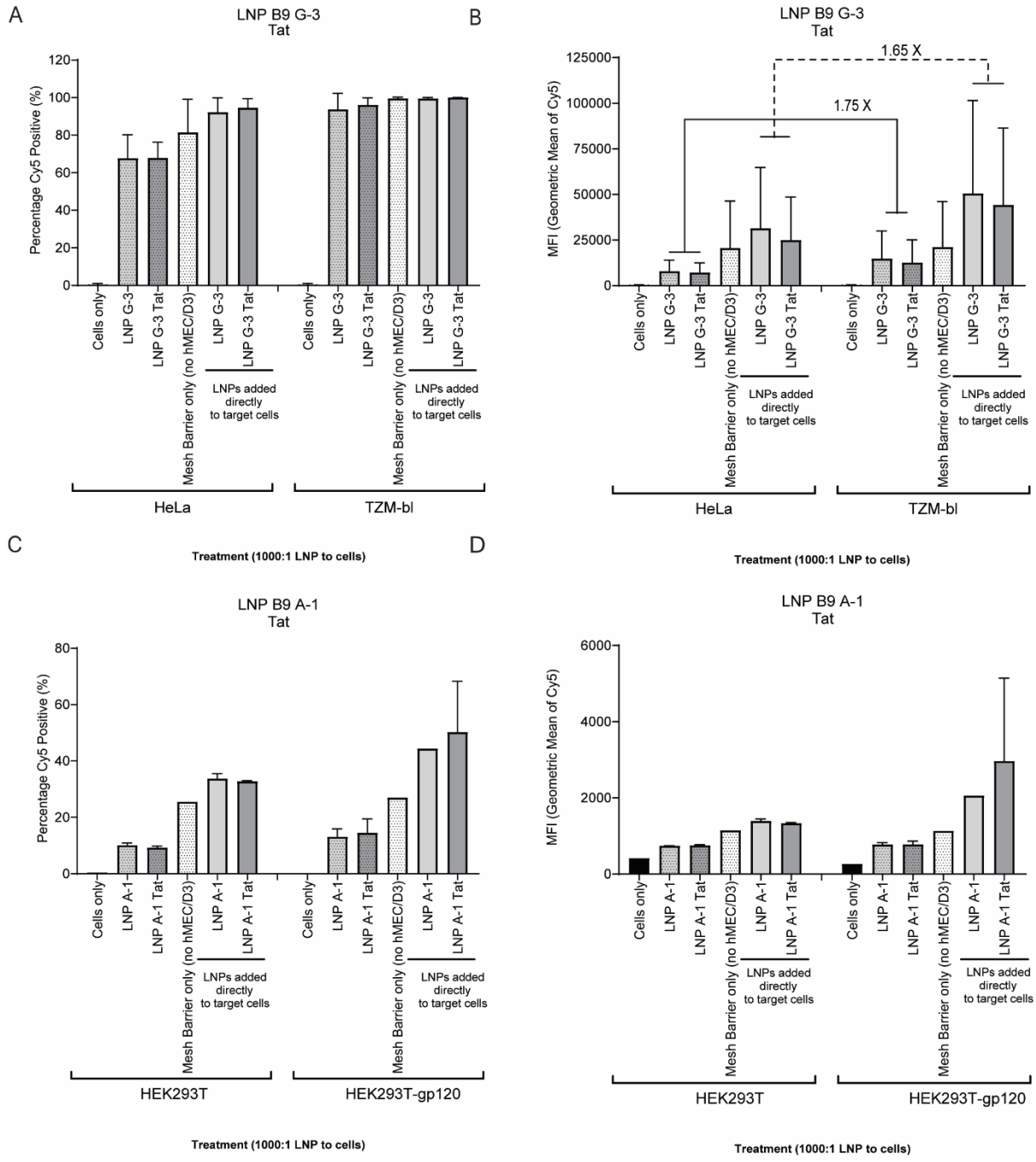

through the hCMEC/D3 barrier or through direct addition, suggesting that it may not be an ideal candidate moving forward.

Figure 2: LNPs with Tat pass through the transwell cell barrier and are taken up by target cells. (A) Percentage cells positive for Cy5 detection in HeLa and TZM-bls (B) Mean fluorescent intensity of Cy5 in each cell population in HeLa and TZM-bls. (C) Percentage cells positive for Cy5 detection in HEK cell types. (D) Mean fluorescent intensity of Cy5 in each cell population in HEK cell types. Histograms are representative of two independent biological experiments, each containing duplicate technical replicates.

LNPs do not stimulate an immune response

In order to further characterize LNPs we decided to evaluate their immunogenic profile. We stimulated monocytes obtained from whole blood for 6 days with 10 ng/mL granulocyte-macrophage colony-stimulating factor (GMCSF). This programs the monocytes to form macrophages that are primed to respond in a type 1 manner. After 24 hrs of stimulation with either the LNPs or positive controls for an RNA/DNA response (poly I:C) or a bacterial response (LPS), we found that the LNPs did not increase secretion of any of the cytokines tested (IL-1β, IL-10, IL-6, IFN-ɣ, TNFα, IL-2, IL-4, IL-8 and IL-5) above basal (PBS) conditions (**Figure 3A**). Additionally, we confirmed LNP uptake by the monocyte-derived macrophages (MDMs) using fluorescent microscopy (**Figure 3B**). We found that all LNPs containing the Cy5 oligonucleotide were observable under the microscope (**Figure 3B**), and that all macrophages were 100% positive for Cy5. Additionally, using QuPath analysis software we determined the Cy5 MFI for each image. Interestingly, we found that the LNP A-1 and the LNP G-3 had higher MFIs in all the donors assessed compared to their Tat and T7 counterparts (**Figure 3C**). Further, we found that the LNP G-3 exhibited the highest uptake in all the donors assessed (**Figure 3C**). These

observations suggest that the candidate LNPs are relatively immunologically inert and may prove to be well-tolerated *in vivo*.

Figure 3

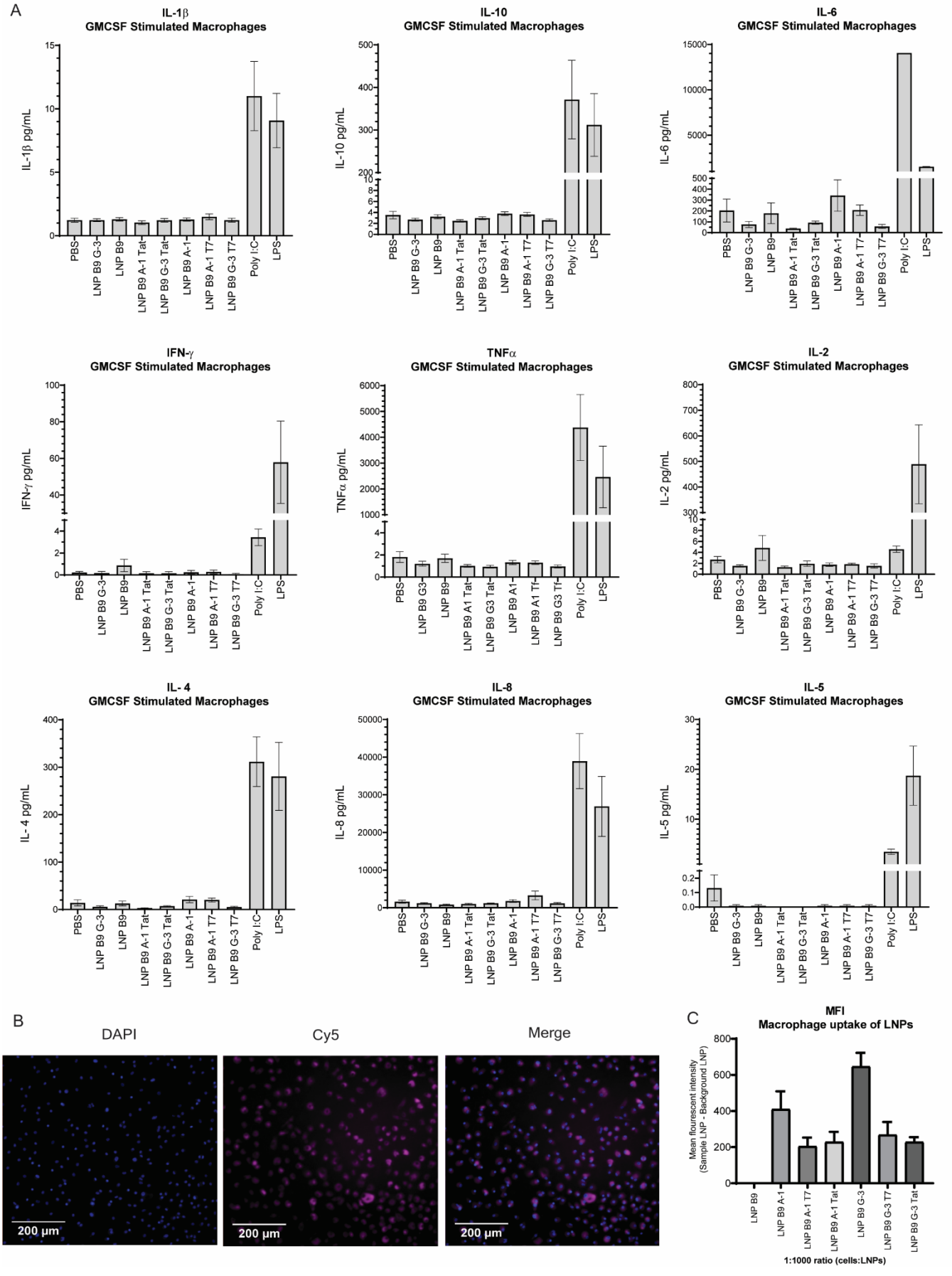
A
IL-1β
GMCSF Stimulated Macrophages
IL-1β pg/mL
IL-10
GMCSF Stimulated Macrophages
IL-10 pg/mL
IL-6
GMCSF Stimulated Macrophages
IL-6 pg/mL
IFN-γ
GMCSF Stimulated Macrophages
IFN-γ pg/mL
TNFα
GMCSF Stimulated Macrophages
TNFα pg/mL
IL-2
GMCSF Stimulated Macrophages
IL-2 pg/mL
IL- 4
GMCSF Stimulated Macrophages
IL- 4 pg/mL
IL-8
GMCSF Stimulated Macrophages
IL-8 pg/mL
IL-5
GMCSF Stimulated Macrophages
IL-5 pg/mL
PBS
LNP B9 G-3
LNP B9
LNP B9 A-1 Tat
LNP B9 G-3 Tat
LNP B9 A-1
LNP B9 A-1 T7
LNP B9 G-3 T7
Poly I:C
LPS
B
DAPI
Cy5
Merge
200 µm
C
MFI
Macrophage uptake of LNPs
Mean flouresecent intensity
(Sample LNP - Background LNP)
LNP B9
LNP B9 A-1
LNP B9 A-1 T7
LNP B9 A-1 Tat
LNP B9 G-3
LNP B9 G-3 T7
LNP B9 G-3 Tat
1:1000 ratio (cells:LNPs)

Figure 3: LNPs do not stimulate secretion of pro-inflammatory cytokines. (A) GMCSF primed MDMs were treated with LNPs at a ratio of 1000 LNPs :1 cell or with poly I:C or LPS for 24 hrs. Thereafter supernatants were harvested, clarified and processed for cytokine detection by Luminex. Analytes included IL-1β, IL-10, IL-6, IFN-ɣ, TNFα, IL-2, IL-4, IL-8 and IL-5. Histograms are representative of three biological experiments, each containing duplicate technical replicates. (B) Representative fluorescent images (DAPI, Cy5, and merged) of macrophages and LNP G-3 after 24 hrs. All macrophages were 100% positive for LNP uptake independent of aptamer and peptide composition, however (C) MFI analysis using QuPath v.0.2.2 suggests that the LNP G-3 had the highest uptake compared to the other LNP formulations in type 1 MDMs.

Aptamer and peptide LNPs have modest effects on cell viability in a cell specific manner

We next assessed whether LNPs could affect cell viability in HeLa and HEK293Ts. Cells were treated with the LNPs for 24 hr prior to performing the alamarBlue viability assay. In HeLa cells, we found that the LNP B9 alone had no effect on cell viability compared to the PBS control (**Figure 4A**). Interestingly, we observed that cell viability was reduced by ~20% in HeLa cells treated with LNPs containing either A-1 or G-3 aptamer or LNPs with the Tat or T7 peptide alone (**Figure 4A**). However, LNPs containing both the aptamer and a peptide (Tat or T7) did not further affect cell viability (**Figure 4A**). This suggests that the aptamer and the peptides may contribute towards the loss of cell viability observed in this cell type. Conversely, we observed no loss of cell viability in HEK293T cells treated with LNPs containing either A-1 or G-3 aptamer, Tat or T7 alone, or the combination of aptamers and peptides (**Figure 4B**). Like HeLa cells, the LNP formulation alone had no effect on cell viability (**Figure 4B**). These data suggest that there

may be some cell specific sensitivity toward the LNPs formulations, and that further studies are required to determine the optimal concentrations of aptamers and peptides within the LNPs, or to optimize the ratio of LNPs to cells in order to reduce toxicity in any cell line tested.

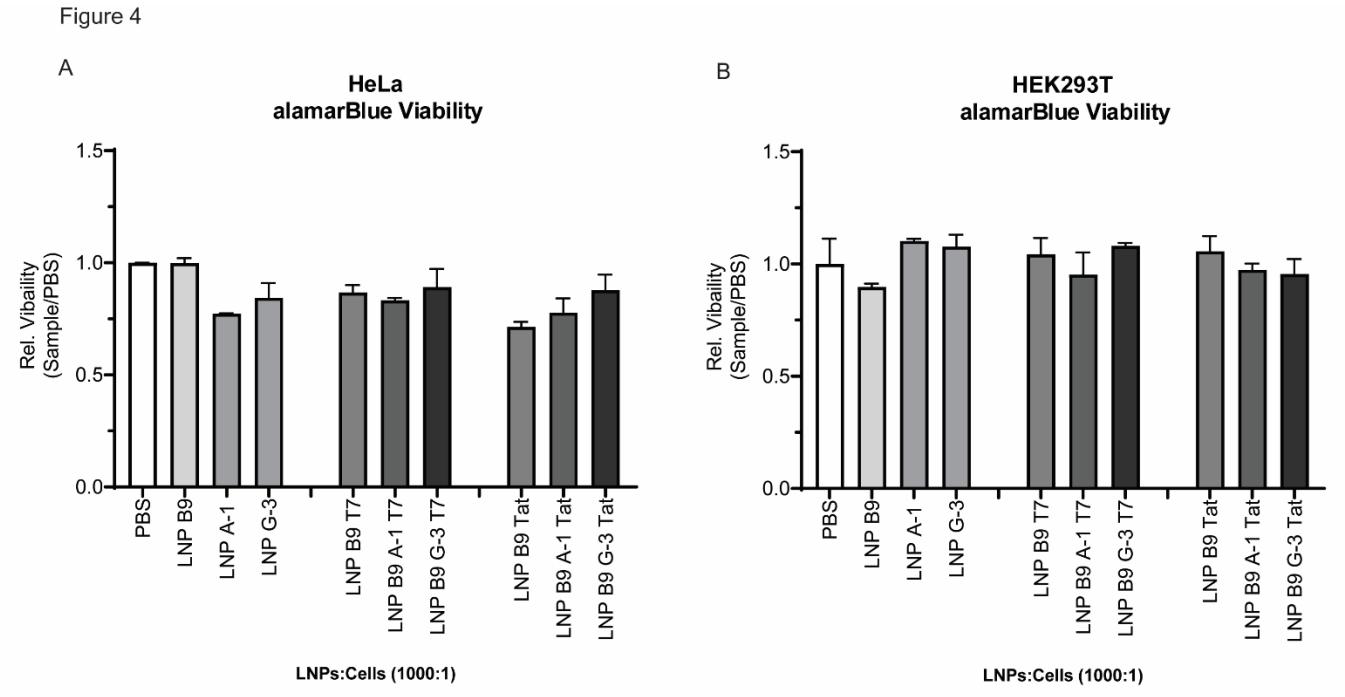

Figure 4: LNPs modestly affect cell viability in a cell specific manner. HeLa (A) or HEK293T (B) cells were treated overnight with the LNPs at a ratio of 1000:1. Next, the alamarBlue viability assay was performed and viability as fraction of control (PBS) was determined. Histograms are representative of the mean ±SEM. Data representative of two independent experiments performed in quadruplicate.

Discussion

LNPs represent an increasingly popular modality for cargo delivery. The vast improvements in lipid design and architecture have resulted in several successful LNP-driven vaccines and

therapeutics including two RNA-based SARS-CoV-2 vaccines [43], as well as an siRNA-LNP for the treatment of a transthyretin amyloidosis [36]. However, further improvements in toxicity profiles, cargo-delivery and cell or organ specificity are needed to expand the use of LNPs for gene and drug delivery.

LNPs and aptamers have previously been used with great success to increase cell specificity. Liang et al., (2015) reported on a novel aptamer-LNP targeting osteoblasts. The authors conjugated aptamers to a PEG-DSPE and observed that their LNP-DNA aptamer was able to deliver target siRNA into osteoblasts via macropinocytosis thereby to increase bone formation *in vitro* and in rodents [44]. Kim et al., (2017) used a post-insertion method to incorporate an aptamer-maleimide-PEG into their LNPs to target *EGFR* positive cancer cells. The authors showed an increased delivery of siRNAs and fluorescent quantum dot nanocrystals both *in vitro* and in *EGFR* positive tumor xenografts in mice [45]. Chandra et al., (2020) used a maleimide-PEG in their LNP formulation to functionalize their LNPs with an aptamer specific for the HER2 receptor. Here, functionalized LNPs increased siRNA delivery and subsequent sensitivity of the doxorubicin-resistant HER2 positive breast cancer cell lines by ~2 fold over LNPs with no aptamers [46]. Taken together, work reported by these authors, as well as others, demonstrates usefulness of aptamers to increase cellular specificity and uptake of LNPs into the target cells. In the present study, we observed that LNPs containing the G-3 aptamer targeting CCR5 resulted in a 40% increase in cellular uptake through the BBB and into target cells, and that these cells had higher LNP uptake (measured by a higher MFI) than their non-antigen expressing counterparts; while the gp160 aptamer (A-1) had no apparent effect on target cell uptake. One could speculate that this may be the result of the nature of the target proteins. CCR5, a cell surface receptor, is internalized upon ligand binding, before recycling back to the cell surface or processed for degradation in the lysosome [34]. On the other hand, gp120 is a viral surface

protein that is involved in viral entry through complexation with CD4 and CCR5 or CXCR4 host cell surface receptors [35]. As such, gp160 expression on the host cell surface receptor, may not be as adept at facilitating cell entry via receptor-mediated endocytosis. Although Zhou et al., (2009), observed by confocal microscopy that the A-1 aptamer entered gp160-positive cells and suggested that receptor-mediated endocytosis could be mechanism of entry, such a notion was not definitively demonstrated as the mechanism of uptake [35]. In addition, observed differences between these aptamers could also be due to differences in target receptor expression in the cell types, and/or differences in the affinity and specificity of these aptamers for their target receptors and/or differences in their mechanisms of uptake. Finally, the formulation procedure also likely influences the ability of the aptamers to act as productive ligands for their respective receptors, although more studies will be needed to fully delineate these effects.

One important aspect we set out to address was to identify proxies for successful LNP-mediated cargo delivery through the BBB and into the brain. As previously stated, effective transport systems for brain drug delivery are highly warranted. Herein, we find that the LNP platform can be applied as a vehicle to circumvent the BBB and effectively deliver oligonucleotide probes to antigen-expressing cell lines. In the case of HIV-1, there is currently a need for more effective delivery platforms compatible with anti-retroviral drugs. Specifically, a productive CNS delivery of such compounds is expected to reduce HIV-1 associated neurological disorders as well as to reduce HIV-1 replication at this sanctuary site [13, 47, 48].

We investigated the use of T7 and Tat peptides and evaluated their ability to aid delivery of LNP-aptamer species across the BBB. We found that LNPs with either T7 or the Tat peptide did not significantly increase cellular uptake through the BBB above the LNPs containing aptamers alone. T7 appeared to have an effect on cellular uptake when the LNPs were directly added to the cells, and a small effect when applied through the apical chamber of the hCMEC/D3 cell line,

while Tat had no effect. It may be prudent to dose the amount of post-inserted Tat or T7 peptide used in these formulations. For example, Duchardt et al, (2007), used 2-40 μM Tat peptide as a cell penetrating peptide to facilitate siRNA entry. In particular, the authors observed that clathrin-dependent endocytosis increased with increasing concentrations of Tat peptide, suggesting that high concentrations may be needed to elicit an effective endocytosis mechanism [18]. Qin et al., (2011) conjugated Tat to PEG_{2000} and found that in their liposomal formulations, those containing 10% PEG_{2000}-Tat had the most efficient uptake in a BBB model [9]. Several studies have used transferrin-conjugated PEG analogs. Pang et al., (2011) in a series of papers observed that liposomes comprised of 5 – 10% PEG-transferrin increased brain delivery by 2.8 fold compared to their liposomes without transferrin in a BBB model and *in vivo* [15], and further when loaded with the chemotherapeutic agent doxorubicin, observed increased delivery of this compound and subsequently a significant tumor regression in mouse xenografts [22]. Kircheis et al., (1997; 2002) developed a polyethyleneimine (PEI)-conjugated transferrin molecule at a ratio of 21.4 nmol PEI: 270 nmol transferrin, and observed that transferrin shielded the PEI, decreasing toxicity and increasing target cell uptake through binding to the transferrin receptor both *in vitro* and *in vivo* [49, 50]. In the work presented here, we immobilized Tat or transferrin onto the LNP formulations using a post-insertional technique. It could be that it would be more prudent to make the LNP formulation with the addition of Tat and T7 peptide during the initial synthesis.

Further, it may be important to increase the amount of post-insertional Tat and T7 used in future experiments, considering the concentrations we used were relatively low (~0.1% post addition). Another approach is to use next generation of short peptides that also bind to the transferrin receptor at non-competing regions to endogenous transferrin *in vivo* [51]. These molecules are known as cystine dense peptides (CDPs), and have been shown to bind to the transferrin receptor in the picomolar range to facilitate BBB crossing in mouse models [51]. These short

peptides may be advantageous to use when approaching an *in vivo* strategy especially considering that the concentration of the peptide needed in the formulation may be lower compared to the T7 peptide used in this study; however, its safety profile must still be fully evaluated.

Nevertheless, our LNPs, particularly the ones containing the G-3 aptamer alone resulted in BBB transport ranging from 50–65% in non-target cell lines, to 80–100% uptake in target cell lines. Importantly, the hCMEC/D3 model represents a simplified representation of the BBB, which does not account for the full complexities of the BBB *in vivo* [52, 53]. One could perform more complex *in vitro* assays that include a multicellular reconstruction of the BBB to also include astrocytes and microglial cells [54, 55]. However, it may be more effective to perform further studies in non-primate animal models to determine the efficacy of these LNPs in passing through the BBB. Assessing and quantitating the percentage of LNP B9 to traverse the BBB is a critical step to determining its use as an effective LNP able to deliver small molecules or oligonucleotides into the brain. One important caveat to note is that the aptamers are species specific, thus the use of a xenograft model with human cells in a non-primate animal models are needed to determine the specificity of the LNP-aptamer tested.

Furthermore, while the LNP B9 alone had no effect on cellular viability, it appeared that the LNPs containing either the A-1 or G-3 aptamers, or the peptides, reduced cellular viability in HeLa cells by 20%, suggesting that there may be some toxicity when delivered to cells. However, these effects were not observed in HEK293T cells. It could be that the HeLa cell line is more sensitive than the HEK293T cell line. Nevertheless, the data suggest that further testing is required to determine the safety profile of these LNP aptamer and or peptide formulations. One way we could reduce the toxicity profile, is to chemically modify the RNA aptamers [33, 56, 57, 58], or by reducing the aptamer concentration per LNP to thereby alleviate some of the observed the

cellular toxicity. It could be that the RNA aptamer itself could contribute towards cell death, possibly through stimulating the retinoic acid-inducible gene 1 (RIG-1) pathway, and it may thus be prudent to assess IFN-α and IFN-β in the future [32, 59]. Importantly, the LNP B9 formulation alone had no effect on cell viability, suggesting that the ratio of cationic and ionizable lipids is optimal and does not present acute toxicity issues. However, more work is needed to assess its toxicity *in vivo,* and in particular evaluate its effect on the liver [60]. Importantly, LNPs reported herein did not appear to stimulate an immune response in primary human monocyte-derived macrophages. Further, the addition of the aptamers and or the peptides in the LNP formulations had no effect on immune stimulation, suggesting that these LNPs and their modifications may be well tolerated *in vivo*. Importantly, both IL-6 and IFN-ɣ cytokines were not stimulated after exposure to the LNPs, suggesting that this LNP formulation may not induce cytokine release syndrome *in vivo* [60, 61].

Taken together, we have shown that the LNP B9 formulation is safe, can traverse the BBB and is readily taken up in multiple cell types. In the future it will be interesting to explore whether increased uptake may also lead to increased delivery of target molecules such as siRNA, mRNA or small molecules. Further, having LNPs that are specific for HIV-1 infected cells or HIV-1 target cells, may help to facilitate HIV-1 drug treatment to regions of poor drug accessibility like the brain. More effective delivery of antiretroviral drugs may help to reduce HIV-1 associated neurological disorders that are present in HIV-1 positive individuals, as well as reduce populations of HIV-1 positive cells that are poorly accessible through current systemic drug treatment strategies.

Experimental

Materials

(6*Z*,9*Z*,28*Z*,31*Z*)-Heptatriaconta-6,9,28,31-tetraen-19-yl 4-(dimethylamino)butanoate (DLin-MC3-DMA, >98%) was purchased from D&C Chemicals (China), 1,2-distearoyl-*sn*-glycero-3-phosphocholine (DSPC) and cholesterol (Chol) were purchased from Echelon Biosciences, Inc. (USA), and 1,2-dimyristoyl-*rac*-glycero-3-methoxypolyethylene glycol-2000 (DMG-PEG 2000) was purchased from Avanti Polar Lipids, Inc. (USA). Ethanol (BioUltra, ≥99.8%), citric acid monohydrate, sodium chloride, Na_2HPO_4, and KH_2PO_4 were purchased from was purchased from Sigma–Aldrich (Germany).

RNA and DNA oligonucleotides

The RNA aptamers and Cy5 DNA oligonucleotides were synthesized at the RNA/DNA synthesis core at City of Hope (Duarte, CA). The RNA aptamers, A-1 [35] and G-3 [34] were developed by Dr Jiehua Zhou at the City of Hope (Duarte, CA). Annealing of the Cy5 DNA oligonucleotide to the RNA aptamers was confirmed using an electromobility shift assay (EMSA), using an 8% TBE gel (Novex™ , Thermofisher Scientific, MA), under native conditions (**Supplementary Figure 1A**).

RNA aptamers:

GP160: (GGG AGG ACG ATG CGG AAT TGA GGG ACC ACG CGC TGC TTG TTG TGA TAA GCA GTT TGT CGT GAT GGC AGA CGA CTC GCC CGA XXX XXX GTA CAT TCT AGA TAG CC)

CCR5: (GGG AGG ACG ATG CGG GCC TTC GTT TGT TTC GTC CAC AGA CGA CTC GCC CGA XXX XXX TGA TAG ATT GAT AGA)

Complementary DNA:

A-1: (Cy5/AGG CTA TCT AGA ATG TAC)

G-3: (Cy5/TCT ATC AAT CTA TCA)

Peptide synthesis, purification and characterization

Peptide assembly was carried out by SPPS strategy in standard SPE filtration columns. Initially, Fmoc group removal from the Rink linker was achieved by applying 20% piperidine in DMF (2 x 30 min). Preactivation of Fmoc amino acid (4 equiv) prior each coupling was performed with 1-[bis(dimethylamino)methylene]-1*H*-1,2,3-triazolo[4,5-*b*]pyridinium 3-oxid hexafluoro-phosphate (HATU) (4 equiv) and *N*,*N*-diisopropylethylamine (DIPEA) (6 equiv) in DMF. Then the activated mixture was added to the resin swollen in DMF and manual stirring was applied approximately every 15 min over a total reaction time of 2 h. The first amino acid was installed via double coupling. Fmoc deprotection was achieved via 20% piperidine in DMF (1 x 2 min and 1 x 18 min) to prepare the resin for the next coupling step. The resin was washed three times with each solvent in the given order DMF, DCM and DMF after every reaction step.

Peptide sequences:

T7: H-HAIYPRH-NH_2

Modified T7: dipalmitoyl-Dap-HAIYPRH-NH_2

Tat: H-YGRKKRRQRRR-NH_2

Modified Tat: dipalmitoyl-Dap-YGRKKRRQRRR-NH_2

Peptide conjugation with a lipid reagent

The peptides were N-terminally modified on solid support by coupling of Fmoc-Dap(Fmoc)-OH, followed by the coupling of palmitic acid to afford the complete peptide-lipid conjugates. Coupling of Fmoc-Dap(Fmoc)-OH and Fmoc deprotection were carried out as described above. To ensure the complete lipidation of the two free amines of Dap, 8 equiv. of palmitic acid, 8 equiv. of HATU and 12 equiv of DIPEA in DMF was used. Cleavage of the peptide-lipid conjugates from the solid support and removal of the side chain protecting groups was achieved by using trifluoroacetic acid (TFA)/phenol/water/triisopropyl silane (TIPS) = 88:5:5:2 (3 x 60 min). After

cleavage, the remaining resin was extracted with DCM (2 x 10 min). All DCM extracts and TFA cleavages were combined and the resulting mixture was reduced under nitrogen flow. The received solid product was dissolved in DCM and subsequently reduced under nitrogen flow. This procedure was repeated two more times, followed by a lyophilization step to receive the crude peptide. The crude T7-lipid conjugate was purified by normal phase chromatography utilizing gradient elution (2-50% MeOH in DCM). The desired modified T7 peptide was characterized via MALDI-TOF spectrometry (Bruker, MA) (**Supplementary Figure 1B**) and isolated as a colorless powder (9 mg, 6 μmol, 6% yield). $[M+H]^+$ calc. 1455.00, $[M+H]^+$ found. 1455.20. The crude Tat-lipid conjugate was precipitated from DMF as a white power and used without further purification. The modified Tat peptide was characterized via MALDI-TOF spectrometry (**Supplementary Figure 1C**) (31 mg, 14 μmol, 15% yield) $[M+H]^+$ calc. 2121.48, $[M+H]^+$ found. 2121.17.

Lipid nanoparticle synthesis

The formulation protocol was largely adapted from Jayaraman et al, (2012) [4]. Freshly prepared lipid stocks (in chloroform) were mixed to obtain the desired mole fractions (DLin-MC3-DMA/DSPC/Cholesterol/DMG-PEG 2000, 0.4:0.1:0.4:0.1) and the lipid mixture was concentrated under vacuum. The lipid film was dissolved in ethanol (20.3 mg/mL) and added dropwise to stirring 50 mM citrate buffer pH 4.0, pre-heated to 35 °C to get a final lipid concentration of 6.1 mg/mL. The lipid solution was stirred for an additional 20 min at 35 °C, after which the lipid solution was allowed to slowly reach rt, transferred to a 1 mL Hamilton syringe, and extruded 10 times at rt through two 100 nm Nucleopore membrane filters (Whatman) using Avanti Mini Extruder (Avanti Polar Lipids, Inc., USA).

Complementary oligonucleotides GP160:A-1 (1.4 nmol, 30 μL 1x PBS pH 7.4) and CCR5:G-3 (1.4 nmol, 30 μL 1x PBS pH 7.4) underwent annealing (85 °C for 10 min, 25 °C for 20 min, +4

°C for 20 min). GP160:A-1 (30 μL) and CCR5:G-3 (30 μL) were each added to a stirring LNP suspension (6.1 mg/mL, 165 μL) pre-heated to 35 °C, and LNP-DNA lipoplex suspensions were further diluted with 50 mM citrate buffer pH 4.0, 30% EtOH (120 μL) to get a final lipid concentration of 3.2 mg/mL and a DNA/lipid ratio of roughly 0.05 (wt/wt). The LNP-DNA lipoplexes were allowed to form over 30 min at 35 °C (no stirring). Buffer exchange was performed using 3K Amicon Ultra-0.5 Centrifugal Filter Unit (Merck Millipore, USA) providing the final LNP-DNA lipoplexes in 1x PBS pH 7.4 (3 mg/mL final lipid concentration). Post insertion of peptides was carried out by diluting the peptides to a final concentration of 1.7 μg/mL Tat lipid and 3.0 μg/mL T7 lipid in 1x PBS pH 7.4. Thereafter, diluted lipopeptides (18 μL T7, 31.8 μL Tat) were added to the LNPs (90 μL). Samples were incubated on a thermomixer for 30 minutes (25°C at 250 rpm) for post-insertion addition. Thereafter samples were stored at 4°C until further use.

Dynamic light scattering and Zeta potential

Particle size, polydispersity and zeta potential were analyzed by dynamic light scattering instrument model Zetasizer Nano ZS (Malvern Instruments, Malvern, UK) having He-Ne 633 nm laser at an angle of detection of 90° with incubation time of 60 s. Samples were diluted 50-fold in Milli-Q water and placed into in the disposable plastic cuvettes for measurement performed in triplicates ($n \geq 3$) to obtain a mean value.

Nanoparticle tracking analysis (NTA)

Concentration and size of LNPs with and without peptides were additionally confirmed using the NanoSight NS300 (Malvern Panalytical, United Kingdom), using the Nanoparticle Tracking Analysis (NTA) software (version 3.44, Malvern Panalytical, United Kingdom). Samples were run at a 1:1000 dilution, with three technical replicates per sample. A blue488 laser was used to

detect the LNPs, with a slide shutter level set to 1232 and the slider gain set to 219, and the syringe pump speed set to 30 using a flow-cell top plate module.

Cell lines and maintenance

HeLa and HEK293T were purchased from American Type Culture Collection (ATCC, VA). TZM-bls were acquired through the NIH AIDS reagent program and were engineered to express high levels of the HIV-1 co-receptor CCR5 [62]. HEK293T-gp160 cells were a kind gift from Dr. Bing Chen (Harvard, MA), and stably express the 92UG037.8 strain of the viral envelope protein, Env [63]. The human brain endothelial cell line hCMEC/D3 was purchased from Millipore Sigma (MA).

HeLa, TZM-bls, HEK293T and HEK293T-gp160 cell lines were all cultured in Dulbecco's Modified Eagle's Medium (DMEM, Corning™, NY) in 10% FBS (GeminiBio, CA). hCMEC/D3 cell line was maintained in EndoGRO-MV Complete culture media (Millipore Sigma, MA) on collagen (Collagen Type 1, rat tail, Millipore Sigma, MA) coated flasks. hCMEC/D3 cells were cultured to a maximum of 10 passages to ensure proper tight junction formation. All cells were maintained in a water-jacket incubator at 37°C. All cell lines were routinely tested and found negative for mycoplasma.

Inflammation assay

Blood from consented and de-identified donors was used in this study under an approved IRB 19582 (City of Hope, Duarte, CA). To obtain monocytes we followed the methodology by Menck et al., 2014 [64]. Briefly, blood was initially processed using a Histopaque®-1077 (Millipore Sigma, MA) density separation to collect the buffy coat. Thereafter, the buffy coat was subject to a Percoll® (Cytiva, MA) density separation to enrich for the monocyte population in the buffy coat. Monocytes were counted and stored in Cyrostor-C5 (BioLife Solutions, WA) at -80°C until further use. Monocytes were plated at a density of 1 X 10^5 cells per 96 well plate, and stimulated

for 6 days with 10 ng/mL GM-CSF (Gibco™, ThermoFisher Scientific, MA) in RPMI (Corning™, NY) supplemented with 5% FBS, 1% AB normal human serum (Millipore Sigma, MA) and 1% penicillin/streptomycin (Millipore Sigma, MA). Media was replaced every 3 days. After 6 days, media was replaced without GM-CSF and LNPs (Ratio 1000:1), Poly I:C (25 µg/mL, Millipore Sigma, MA) or LPS (1 µg/mL, Millipore Sigma, MA) was added to the macrophages. Twenty-four hours later, supernatant was collected and centrifuged at 300 *X g* for 5 minutes to remove cellular debris. Harvested supernatant was stored at -80°C until processed for cytokine expression using a 10-Plex Human Cytokine Panel (LHC6004M, ThermoFisher Scientific, MA). The Luminex assay was processed on a Luminex® 200 machine (Luminexcorp, TX) by the Analytical Pharmacology Core (City of Hope, Duarte, CA).

Transwell Assay

The transwell assay was adapted from Weksler et al, (2005) [53]. Briefly, hCMEC/D3 were cultured on pre-soaked 0.4 µM transwell-filters (Greiner Bio-One Thincert™ CellCoat™, Austria) at a density of 5 X 10^4 cells/cm^2 in a 24 well culture dish. After 6 hours, media was removed from the apical chamber and replaced with 200 µL fresh EnoGRO-MV complete culture media (Millipore Sigma, MA). The basolateral chamber was filled with 600 µL media. The next day, the media was changed to a low supplement EGM-2 basal medium (Lonza Walkerville, MD) supplemented with 2.5% FBS, 0.55 µM hydrocortisone (Stemcell Technologies, Canada), 1% Penicillin/streptomycin (Millipore Sigma, MA) and 10 mM HEPES (Gibco™, Thermofisher Scientific, MA). The culture was maintained, and media replaced every 2nd day until a trans-endothelial electrical resistance (TEER) of ~30 Ω.cm^2 was reached. TEER was measured using an EVOM2 with a chopstick electrode (World Precision Instruments, FL). Resistivity was calculated using the formula:

$$Resistivity\ (\Omega.cm^2) = (Sample\ \Omega - Control\ \Omega) \times surface\ area\ of\ insert$$

Once the integrity of the barrier was assessed, the apical transwell chambers were transferred to new 24 well culture dishes with 50,000 cells per well of HeLa, TZM-bl, HEK293T or HEK293T-gp160 cells that had been plated 24 hrs previously. LNPs at a ratio of 1000: 1 cell was added to each well. Twenty-four hours later, the apical layer was removed, and the basolateral cells were washed, trypsinized and resuspended in 1 X PBS. Detection of Cy5 was measured by flow cytometry on a BD Accuri™ C6 (Becton, Dickinson and Company, NJ) and data was analyzed using FlowJo™ version 10.7.1 (Becton, Dickinson and Company, NJ). Cells were first gated on FFC-A vs. SSC-A followed by SSC-H vs. SSC-A to gate on single cells, before designating negative and positive population gates using a histogram.

Viability Assay

The alamarBlue assay was performed according to the manufacturer's instructions (ThermoFisher Scientific, MA). Briefly, 10,000 HeLa cells and 40,000 HEK293T cells were seeded in a 96 well plate. The next day, LNPs at a ratio of 1000:1, were added to the cells. Twenty-four hours later, 0.1 volume of 10X alamarBlue was added and the cells incubated for 1 hr at 37°C. Fluorescence was measured on a GloMax® Explorer multimode microplate reader (Promega, WI). Background measurements from a media only control was subtracted from all the measurements before calibrating to the PBS control.

Light microscopy

To assess tight junction formation, we adapted the protocol from Vu et al., 2009 [52]. Briefly, the apical chamber was washed with 1 X PBS and fixed with ice-cold 4% paraformaldehyde for 15 minutes at 4°C before washing 2X with ice-cold PBS. The chambers were blocked with 1% BSA-PBS for 60 min at 4°C and subsequently incubated overnight at 4°C with Claudin 5 – Alexa Fluor 488 (cat # 35-258-8, ThermoFisher Scientific, MA) at 5 µg/mL in 1% BSA-PBS. Thereafter, cells were washed 3X with ice-cold PBS. The membrane was subsequently cut out of the insert with a scalpel

blade and using tweezers, placed on a slide and air dried. Once dried, a small drop of Diamond Anti-Fade Mountant with DAPI (Invitrogen™, ThermoFisher Scientific, MA) was added and a coverslip placed over the membrane. Slides were cured overnight at 4°C before being visualized using a Zeiss Axio Vert A.1 light microscope with a Zeiss AxioCam 503 color camera (Carl Zeiss Microscopy GmbH, Germany). Images were processed using ZEN blue software (version 2.3, Carl Zeiss Microscopy GmbH, Germany), and merged using ImageJ version 1.53a (Wayne Rasband, NIH, USA).

To assess uptake of the LNPs in primary macrophages, samples were washed 1 X with PBS and fixed with 4% with ice-cold 4% paraformaldehyde (in PBS), for 15 minutes at 4°C. The formaldehyde was removed, and the cells washed 2X with ice-cold PBS. Thereafter, PBS containing DAPI (10 ng/mL) was added and the cells visualized using a Zeiss Observer II light microscope with a Zeiss AxioCam 506 Mono camera (Carl Zeiss Microscopy GmbH, Germany). Images were acquired using the ZEN blue software (Version 2.3, Carl Zeiss Microscopy GmbH, Germany). Images were processed using ImageJ version 1.53a (Wayne Rasband, NIH, USA). To analyze the mean fluorescent intensity, we used QuPath version 0.2.2 [65] (The University of Edinburgh, UK). We analyzed two different fields of view per treatment group for each donor (n = 3). For the analysis we used the positive cell detection software with the following parameters: detection channel set to DAPI, with a requested pixel size of 0.45 µm. Nucleus parameters were set to a background radius of 8 µm, a media filter radius of 1 µm, a sigma value of 3 µm, a minimum area of 10 μm^2 and a maximum area of 400 μm^2. Intensity parameters were set to a threshold of 150. Cell expansion was set to 5 µm. 'Split by shape, Include cell nucleus, Smooth boundaries and Make measurements boxes were all checked. Intensity threshold parameters were set to a single threshold with the score compartment set to cytoplasm: Alexa Flour 647 mean. Mean cytoplasm Alexa Flour 647 values were used and represented as mean ±SEM.

Negative staining electron microscopy of LNPs

Specimens diluted at 1:1000 were absorbed onto glow-discharged, carbon-coated 200 mesh EM grids. Samples were prepared by conventional negative staining with 1% (*w/v*) uranyl acetate. EM images were collected with an FEI Tecnai 12 transmission electron microscope (Thermo Fisher Scientific, MA) equipped with a LaB6 filament and operated at an acceleration voltage of 120 kV. Images were recorded with a Gatan 2×2 k CCD camera (Gatan, Inc., Pleasanton, CA, USA) at a magnification of 21 000 - 26 000 X and a defocus value of ~1.5 µm. TEM images were analyzed using ImageJ version 1.53a (Wayne Rasband, NIH, USA). Briefly, the scale was set to the scale bar on the image, and the diameter for entire nanoparticles was measured in each image. At least 3 images per LNP formulation was used to determine the size distribution of the LNPs. Data are represented as a box and whisker plot, with min and max values representing the error bars.

Statistical analysis

Experiments are representative of two or three biological repeats performed in technical duplicates, unless otherwise stated. Data are represented as histograms with mean ± SEM. Data was prepared and analyzed using GraphPad Prism for Windows version 8.3 (GraphPad Software, CA).

Supporting information available:

Supplementary Figure 1, EMSA and MALDI TOF of oligonucleotides;

Supplementary Figure 2, TEM data for LNPs;

Supplementary Figure 3, hCMEC/D3 cell images;

Supplementary Figure 4, FACS images.

Acknowledgements

Research reported in this publication included work performed by the Electron Microscopy, the RNA/DNA Synthesis and the Analytical Pharmacology Core Facilities at the City of Hope, Duarte, CA. We would like to thank Dr. Zhuo Li and Ricardo Zerda at City of Hope Electron Microscopy core for their help. We would like to thank the Light Microscopy core for the use of their microscopes as well as the Analytical Cytometry core for the use of their flow cytometers (City of Hope, Duarte, CA). The Analytical Pharmacology is supported by the National Cancer Institute of the National Institutes of Health under grant number P30CA033572. The content is solely the responsibility of the authors and does not necessarily represent the official views of the National Institutes of Health. Galina Shevchenko (The Center for Gene Therapy and Irell & Manella Graduate School of Biological Sciences, The Beckman Research Institute, The City of Hope, Duarte CA) is acknowledged for assisting with LNP preparation and tests.

Funding

This project was supported by NIMH R01 113407-01 to KVM and by Villum YIP grant 40851 to KA.

References

1. Kulkarni, J. A.; Cullis, P. R.; van der Meel, R., Lipid Nanoparticles Enabling Gene Therapies: From Concepts to Clinical Utility. *Nucleic Acid Therapeutics* **2018,** *28* (3), 146-157.
2. Rungta, R. L.; Choi, H. B.; Lin, P. J.; Ko, R. W.; Ashby, D.; Nair, J.; Manoharan, M.; Cullis, P. R.; Macvicar, B. A., Lipid Nanoparticle Delivery of siRNA to Silence Neuronal Gene Expression in the Brain. *Molecular therapy. Nucleic acids* **2013,** *2* (12), e136-e136.
3. Zhao, Y.; Huang, L., Lipid Nanoparticles for Gene Delivery. *Advanced Genetics* **2014,** *88*, 21.
4. Jayaraman, M.; Ansell, S. M.; Mui, B. L.; Tam, Y. K.; Chen, J.; Du, X.; Butler, D.; Eltepu, L.; Matsuda, S.; Narayanannair, J. K.; Rajeev, K. G.; Hafez, I. M.; Akinc, A.; Maier, M. A.; Tracy, M. A.; Cullis, P. R.; Madden, T. D.; Manoharan, M.; Hope, M. J., Maximizing the Potency of siRNA Lipid Nanoparticles for Hepatic Gene Silencing In Vivo. *Angewandte Chemie International Edition* **2012,** *51* (34), 8529-8533.
5. Whitehead, K. A.; Dorkin, J. R.; Vegas, A. J.; Chang, P. H.; Veiseh, O.; Matthews, J.; Fenton, O. S.; Zhang, Y.; Olejnik, K. T.; Yesilyurt, V.; Chen, D.; Barros, S.; Klebanov, B.; Novobrantseva, T.; Langer, R.; Anderson, D. G., Degradable lipid nanoparticles with predictable in vivo siRNA delivery activity. *Nature Communications* **2014,** *5*, 4277.
6. Cheng, Q.; Wei, T.; Farbiak, L.; Johnson, L. T.; Dilliard, S. A.; Siegwart, D. J., Selective organ targeting (SORT) nanoparticles for tissue-specific mRNA delivery and CRISPR–Cas gene editing. *Nature Nanotechnology* **2020,** *15* (4), 313-320.
7. Pardi, N.; Tuyishime, S.; Muramatsu, H.; Kariko, K.; Mui, B. L.; Tam, Y. K.; Madden, T. D.; Hope, M. J.; Weissman, D., Expression kinetics of nucleoside-modified mRNA delivered in lipid nanoparticles to mice by various routes. *J Control Release* **2015,** *217*, 345-351.
8. Sago, C. D.; Lokugamage, M. P.; Paunovska, K.; Vanover, D. A.; Monaco, C. M.; Shah, N. N.; Gamboa Castro, M.; Anderson, S. E.; Rudoltz, T. G.; Lando, G. N.; Munnilal Tiwari, P.; Kirschman, J. L.; Willett, N.; Jang, Y. C.; Santangelo, P. J.; Bryksin, A. V.; Dahlman, J. E., High-throughput in vivo screen of functional mRNA delivery identifies nanoparticles for endothelial cell gene editing. *Proc Natl Acad Sci U S A* **2018,** *115* (42), E9944-E9952.
9. Taskova, M.; Mantsiou, A.; Astakhova, K. Synthetic nucleic acid analogues in gene therapy: an update for peptide–oligonucleotide conjugates, ChemBioChem **2017,** *18* (17), 1671-1682.
10. Gonzalez-Carter, D.; Liu, X.; Tockary, T. A.; Dirisala, A.; Toh, K.; Anraku, Y.; Kataoka, K., Targeting nanoparticles to the brain by exploiting the blood–brain barrier impermeability to selectively label the brain endothelium. **2020,** *117* (32), 19141-19150.
11. Guarnieri, D.; Falanga, A.; Muscetti, O.; Tarallo, R.; Fusco, S.; Galdiero, M.; Galdiero, S.; Netti, P. A., Shuttle-mediated nanoparticle delivery to the blood-brain barrier. *Small (Weinheim an der Bergstrasse, Germany)* **2013,** *9* (6), 853-62.
12. Bertrand, L.; Velichkovska, M.; Toborek, M., Cerebral Vascular Toxicity of Antiretroviral Therapy. *Journal of Neuroimmune Pharmacology* **2019**.
13. Osborne, O.; Peyravian, N.; Nair, M.; Daunert, S.; Toborek, M., The Paradox of HIV Blood–Brain Barrier Penetrance and Antiretroviral Drug Delivery Deficiencies. *Trends in Neurosciences* **2020,** *43* (9), 695-708.
14. Rao, K. S.; Ghorpade, A.; Labhasetwar, V., Targeting anti-HIV drugs to the CNS. *Expert Opin Drug Deliv* **2009,** *6* (8), 771-784.

15. Pang, Z.; Gao, H.; Yu, Y.; Chen, J.; Guo, L.; Ren, J.; Wen, Z.; Su, J.; Jiang, X., Brain delivery and cellular internalization mechanisms for transferrin conjugated biodegradable polymersomes. *International journal of pharmaceutics* **2011,** *415* (1), 284-292.
16. Pulgar, V. M., Transcytosis to Cross the Blood Brain Barrier, New Advancements and Challenges. *Frontiers in neuroscience* **2018,** *12*, 1019.
17. Rui, Y.; Wilson, D. R.; Green, J. J., Non-Viral Delivery To Enable Genome Editing. *Trends in Biotechnology* **2019,** *37* (3), 281-293.
18. Duchardt, F.; Fotin-Mleczek, M.; Schwarz, H.; Fischer, R.; Brock, R., A Comprehensive Model for the Cellular Uptake of Cationic Cell-penetrating Peptides. *Traffic* **2007,** *8* (7), 848-866.
19. Fang, S. L.; Fan, T. C.; Fu, H. W.; Chen, C. J.; Hwang, C. S.; Hung, T. J.; Lin, L. Y.; Chang, M. D., A novel cell-penetrating peptide derived from human eosinophil cationic protein. *PloS one* **2013,** *8* (3), e57318.
20. Vivès, E.; Brodin, P.; Lebleu, B., A truncated HIV-1 Tat protein basic domain rapidly translocates through the plasma membrane and accumulates in the cell nucleus. *The Journal of biological chemistry* **1997,** *272* (25), 16010-7.
21. Qian, Z. M.; Li, H.; Sun, H.; Ho, K., Targeted Drug Delivery via the Transferrin Receptor-Mediated Endocytosis Pathway. **2002,** *54* (4), 561-587.
22. Pang, Z.; Gao, H.; Yu, Y.; Guo, L.; Chen, J.; Pan, S.; Ren, J.; Wen, Z.; Jiang, X., Enhanced Intracellular Delivery and Chemotherapy for Glioma Rats by Transferrin-Conjugated Biodegradable Polymersomes Loaded with Doxorubicin. *Bioconjugate Chemistry* **2011,** *22* (6), 1171-1180.
23. Sharma, G.; Lakkadwala, S.; Modgil, A.; Singh, J., The Role of Cell-Penetrating Peptide and Transferrin on Enhanced Delivery of Drug to Brain. *Int J Mol Sci* **2016,** *17* (6), 806.
24. Lee, J. H.; Engler, J. A.; Collawn, J. F.; Moore, B. A., Receptor mediated uptake of peptides that bind the human transferrin receptor. *European journal of biochemistry* **2001,** *268* (7), 2004-12.
25. Liang, M.; Gao, C.; Wang, Y.; Gong, W.; Fu, S.; Cui, L.; Zhou, Z.; Chu, X.; Zhang, Y.; Liu, Q.; Zhao, X.; Zhao, B.; Yang, M.; Li, Z.; Yang, C.; Xie, X.; Yang, Y.; Gao, C., Enhanced blood-brain barrier penetration and glioma therapy mediated by T7 peptide-modified low-density lipoprotein particles. *Drug delivery* **2018,** *25* (1), 1652-1663.
26. Li, Y.; An, C.; Han, D.; Dang, Y.; Liu, X.; Zhang, F.; Xu, Y.; Zhong, H.; Sun, X., Neutrophil affinity for PGP and HAIYPRH (T7) peptide dual-ligand functionalized nanoformulation enhances the brain delivery of tanshinone IIA and exerts neuroprotective effects against ischemic stroke by inhibiting proinflammatory signaling pathways. *New Journal of Chemistry* **2018,** *42* (23), 19043-19061.
27. Etzerodt, T. P.; Trier, S.; Henriksen, J. R.; Andresen, T. L., A GALA lipopeptide mediates pH- and membrane charge dependent fusion with stable giant unilamellar vesicles. *Soft Matter* **2012,** *8* (21), 5933-5939.
28. Gleue, L.; Schupp, J.; Zimmer, N.; Becker, E.; Frey, H.; Tuettenberg, A.; Helm, M., Stability of Alkyl Chain-Mediated Lipid Anchoring in Liposomal Membranes. *Cells* **2020,** *9* (10).
29. Fritz, T.; Voigt, M.; Worm, M.; Negwer, I.; Müller, S. S.; Kettenbach, K.; Ross, T. L.; Roesch, F.; Koynov, K.; Frey, H.; Helm, M., Orthogonal Click Conjugation to the Liposomal Surface Reveals the Stability of the Lipid Anchorage as Crucial for Targeting. **2016,** *22* (33), 11578-11582.
30. Catuogno, S.; Esposito, C. L., Aptamer Cell-Based Selection: Overview and Advances. *Biomedicines* **2017,** *5* (3), 49.
31. Ye, M.; Hu, J.; Peng, M.; Liu, J.; Liu, J.; Liu, H.; Zhao, X.; Tan, W., Generating aptamers by cell-SELEX for applications in molecular medicine. *Int J Mol Sci* **2012,** *13* (3), 3341-3353.

32. Hwang, S.-Y.; Sun, H.-Y.; Lee, K.-H.; Oh, B.-H.; Cha, Y. J.; Kim, B. H.; Yoo, J.-Y., 5′-Triphosphate-RNA-independent activation of RIG-I via RNA aptamer with enhanced antiviral activity. *Nucleic Acids Research* **2011,** *40* (6), 2724-2733.
33. Odeh, F.; Nsairat, H.; Alshaer, W.; Ismail, M. A.; Esawi, E.; Qaqish, B.; Bawab, A. A.; Ismail, S. I., Aptamers Chemistry: Chemical Modifications and Conjugation Strategies. *Molecules* **2019,** *25* (1), 3.
34. Zhou, J.; Satheesan, S.; Li, H.; Weinberg, M. S.; Morris, K. V.; Burnett, J. C.; Rossi, J. J., Cell-specific RNA aptamer against human CCR5 specifically targets HIV-1 susceptible cells and inhibits HIV-1 infectivity. *Chem Biol* **2015,** *22* (3), 379-390.
35. Zhou, J.; Swiderski, P.; Li, H.; Zhang, J.; Neff, C. P.; Akkina, R.; Rossi, J. J., Selection, characterization and application of new RNA HIV gp 120 aptamers for facile delivery of Dicer substrate siRNAs into HIV infected cells. *Nucleic acids research* **2009,** *37* (9), 3094-3109.
36. Zhang, X.; Goel, V.; Robbie, G. J., Pharmacokinetics of Patisiran, the First Approved RNA Interference Therapy in Patients With Hereditary Transthyretin-Mediated Amyloidosis. **2020,** *60* (5), 573-585.
37. Kulkarni, J. A.; Witzigmann, D.; Leung, J.; Tam, Y. Y. C.; Cullis, P. R., On the role of helper lipids in lipid nanoparticle formulations of siRNA. *Nanoscale* **2019,** *11* (45), 21733-21739.
38. Suhr, O. B.; Coelho, T.; Buades, J.; Pouget, J.; Conceicao, I.; Berk, J.; Schmidt, H.; Waddington-Cruz, M.; Campistol, J. M.; Bettencourt, B. R.; Vaishnaw, A.; Gollob, J.; Adams, D., Efficacy and safety of patisiran for familial amyloidotic polyneuropathy: a phase II multi-dose study. *Orphanet journal of rare diseases* **2015,** *10*, 109.
39. Clogston, J. D.; Patri, A. K., Zeta potential measurement. *Methods in molecular biology (Clifton, N.J.)* **2011,** *697*, 63-70.
40. Skoglund, S.; Hedberg, J.; Yunda, E.; Godymchuk, A.; Blomberg, E.; Odnevall Wallinder, I., Difficulties and flaws in performing accurate determinations of zeta potentials of metal nanoparticles in complex solutions—Four case studies. *PloS one* **2017,** *12* (7), e0181735.
41. Masserini, M., Nanoparticles for brain drug delivery. *ISRN Biochem* **2013,** *2013*, 238428-238428.
42. Jefferies, W. A.; Brandon, M. R.; Hunt, S. V.; Williams, A. F.; Gatter, K. C.; Mason, D. Y., Transferrin receptor on endothelium of brain capillaries. *Nature* **1984,** *312* (5990), 162-163.
43. Dong, Y.; Dai, T.; Wei, Y.; Zhang, L.; Zheng, M.; Zhou, F., A systematic review of SARS-CoV-2 vaccine candidates. *Signal Transduction and Targeted Therapy* **2020,** *5* (1), 237.
44. Liang, C.; Guo, B.; Wu, H.; Shao, N.; Li, D.; Liu, J.; Dang, L.; Wang, C.; Li, H.; Li, S.; Lau, W. K.; Cao, Y.; Yang, Z.; Lu, C.; He, X.; Au, D. W. T.; Pan, X.; Zhang, B.-T.; Lu, C.; Zhang, H.; Yue, K.; Qian, A.; Shang, P.; Xu, J.; Xiao, L.; Bian, Z.; Tan, W.; Liang, Z.; He, F.; Zhang, L.; Lu, A.; Zhang, G., Aptamer-functionalized lipid nanoparticles targeting osteoblasts as a novel RNA interference–based bone anabolic strategy. *Nature Medicine* **2015,** *21* (3), 288-294.
45. Kim, M. W.; Jeong, H. Y.; Kang, S. J.; Choi, M. J.; You, Y. M.; Im, C. S.; Lee, T. S.; Song, I. H.; Lee, C. G.; Rhee, K.-J.; Lee, Y. K.; Park, Y. S., Cancer-targeted Nucleic Acid Delivery and Quantum Dot Imaging Using EGF Receptor Aptamer-conjugated Lipid Nanoparticles. *Scientific Reports* **2017,** *7* (1), 9474.
46. Chandra, S.; Michael Nguyen, H.; Wiltz, K.; Hall, N.; Chaudhry, S.; Olverson, G.; Mandal, T.; Dash, S.; Kundu, A., Aptamer-functionalized Hybrid Nanoparticles to Enhance the Delivery of Doxorubicin into Breast Cancer Cells by Silencing P-glycoprotein. *J Cancer Treatment Diagn* **2020,** *4* (1), 1-13.

47. Gong, Y.; Chowdhury, P.; Nagesh, P. K. B.; Rahman, M. A.; Zhi, K.; Yallapu, M. M.; Kumar, S., Novel elvitegravir nanoformulation for drug delivery across the blood-brain barrier to achieve HIV-1 suppression in the CNS macrophages. *Scientific Reports* **2020,** *10* (1), 3835.
48. Nowacek, A.; Gendelman, H. E., NanoART, neuroAIDS and CNS drug delivery. *Nanomedicine (Lond)* **2009,** *4* (5), 557-574.
49. Kircheis, R.; Kichler, A.; Wallner, G.; Kursa, M.; Ogris, M.; Felzmann, T.; Buchberger, M.; Wagner, E., Coupling of cell-binding ligands to polyethylenimine for targeted gene delivery. *Gene Therapy* **1997,** *4* (5), 409-418.
50. Kircheis, R.; Wightman, L.; Kursa, M.; Ostermann, E.; Wagner, E., Tumor-targeted gene delivery: an attractive strategy to use highly active effector molecules in cancer treatment. *Gene Therapy* **2002,** *9* (11), 731-735.
51. Crook, Z. R.; Girard, E.; Sevilla, G. P.; Merrill, M.; Friend, D.; Rupert, P. B.; Pakiam, F.; Nguyen, E.; Yin, C.; Ruff, R. O.; Hopping, G.; Strand, A. D.; Finton, K. A. K.; Coxon, M.; Mhyre, A. J.; Strong, R. K.; Olson, J. M., A TfR-Binding Cystine-Dense Peptide Promotes Blood–Brain Barrier Penetration of Bioactive Molecules. *Journal of Molecular Biology* **2020,** *432* (14), 3989-4009.
52. Vu, K.; Weksler, B.; Romero, I.; Couraud, P.-O.; Gelli, A., Immortalized human brain endothelial cell line HCMEC/D3 as a model of the blood-brain barrier facilitates in vitro studies of central nervous system infection by Cryptococcus neoformans. *Eukaryot Cell* **2009,** *8* (11), 1803-1807.
53. Weksler, B. B.; Subileau, E. A.; Perrière, N.; Charneau, P.; Holloway, K.; Leveque, M.; Tricoire-Leignel, H.; Nicotra, A.; Bourdoulous, S.; Turowski, P.; Male, D. K.; Roux, F.; Greenwood, J.; Romero, I. A.; Couraud, P. O., Blood-brain barrier-specific properties of a human adult brain endothelial cell line. *FASEB journal : official publication of the Federation of American Societies for Experimental Biology* **2005,** *19* (13), 1872-4.
54. Stone, N. L.; England, T. J.; O'Sullivan, S. E., A Novel Transwell Blood Brain Barrier Model Using Primary Human Cells. **2019,** *13* (230).
55. Bagchi, S.; Chhibber, T.; Lahooti, B.; Verma, A.; Borse, V.; Jayant, R. D., In-vitro blood-brain barrier models for drug screening and permeation studies: an overview. *Drug Des Devel Ther* **2019,** *13*, 3591-3605.
56. Lee, Y.; Urban, J. H.; Xu, L.; Sullenger, B. A.; Lee, J., 2'Fluoro Modification Differentially Modulates the Ability of RNAs to Activate Pattern Recognition Receptors. *Nucleic acid therapeutics* **2016,** *26* (3), 173-182.
57. Jørgensen, A. S.; Gupta, P.; Wengel, J.; Astakhova, I. K. "Clickable" LNA/DNA probes for fluorescence sensing of nucleic acids and autoimmune antibodies. *Chemical Communications* **2013**, *49* (91), 10751-10753.
58. Kumar, T. S.; Myznikova, A.; Samokhina, E.; Astakhova, I. K. Rapid genotyping using pyrene− perylene locked nucleic acid complexes. *Artificial DNA: PNA & XNA* **2013**, 4 (2), 58-68.
59. Kohlway, A.; Luo, D.; Rawling, D. C.; Ding, S. C.; Pyle, A. M., Defining the functional determinants for RNA surveillance by RIG-I. **2013,** *14* (9), 772-779.
60. Moss, K. H.; Popova, P.; Hadrup, S. R.; Astakhova, K.; Taskova, M., Lipid Nanoparticles for Delivery of Therapeutic RNA Oligonucleotides. *Molecular Pharmaceutics* **2019,** *16* (6), 2265-2277.
61. Lee, D. W.; Gardner, R.; Porter, D. L.; Louis, C. U.; Ahmed, N.; Jensen, M.; Grupp, S. A.; Mackall, C. L., Current concepts in the diagnosis and management of cytokine release syndrome. *Blood* **2014,** *124* (2), 188-195.
62. Derdeyn, C. A.; Decker, J. M.; Sfakianos, J. N.; Wu, X.; O'Brien, W. A.; Ratner, L.; Kappes, J. C.; Shaw, G. M.; Hunter, E., Sensitivity of human immunodeficiency virus type 1 to

the fusion inhibitor T-20 is modulated by coreceptor specificity defined by the V3 loop of gp120. *J Virol* **2000,** *74* (18), 8358-67.
63. Chen, J.; Kovacs, J. M.; Peng, H.; Rits-Volloch, S.; Lu, J.; Park, D.; Zablowsky, E.; Seaman, M. S.; Chen, B., HIV-1 ENVELOPE. Effect of the cytoplasmic domain on antigenic characteristics of HIV-1 envelope glycoprotein. *Science* **2015,** *349* (6244), 191-195.
64. Menck, K.; Behme, D.; Pantke, M.; Reiling, N.; Binder, C.; Pukrop, T.; Klemm, F., Isolation of human monocytes by double gradient centrifugation and their differentiation to macrophages in teflon-coated cell culture bags. *Journal of visualized experiments : JoVE* **2014,** (91), e51554.
65. Bankhead, P.; Loughrey, M. B.; Fernández, J. A.; Dombrowski, Y.; McArt, D. G.; Dunne, P. D.; McQuaid, S.; Gray, R. T.; Murray, L. J.; Coleman, H. G.; James, J. A.; Salto-Tellez, M.; Hamilton, P. W., QuPath: Open source software for digital pathology image analysis. *Sci Rep* **2017,** *7* (1), 16878.